

Article

# Study of Hidden-Charm and Hidden-Bottom Pentaquark Resonances in the Quark Model

Xinmei Zhu <sup>1</sup>, Yuheng Wu <sup>2</sup>, Hongxia Huang <sup>2,\*</sup> , Jialun Ping <sup>2</sup>  and Youchang Yang <sup>3</sup>

<sup>1</sup> Department of Physics, Yangzhou University, Yangzhou 225009, China; xmzhu@yzu.edu.cn

<sup>2</sup> Department of Physics, Nanjing Normal University, Nanjing 210023, China; 191002007@njnu.edu.cn (Y.W.); jlping@njnu.edu.cn (J.P.)

<sup>3</sup> School of Physics and Electronic Science, Zunyi Normal University, Zunyi 563006, China; yangyc@gues.edu.cn

\* Correspondence: hxhuang@njnu.edu.cn

**Abstract:** Inspired by the LHCb observation of hidden-charm pentaquarks, i.e.,  $P_c(4312)$ ,  $P_c(4440)$ , and  $P_c(4457)$  in the  $J/\psi p$  invariant mass spectrum, a calculation of the  $J/\psi p$  scattering cross-section was performed using the quark-delocalization color screening model. The results show that  $P_c(4312)$  can be identified as a hidden-charm molecular state  $\Sigma_c D$  with  $J^P = \frac{1}{2}^-$ . The two-peak structure can be reproduced around 4450 MeV, which corresponds to  $P_c(4440)$  and  $P_c(4457)$ . They are the resonances molecular states  $\Sigma_c D^*$  of  $J^P = \frac{1}{2}^-$  and  $J^P = \frac{3}{2}^-$ . Moreover, the  $\Sigma_c^* D^*$  of both  $J^P = \frac{1}{2}^-$  and  $J^P = \frac{3}{2}^-$  are possible molecular pentaquarks. Moreover, in the same theoretical frame, the calculation is extended to the  $P_c$ -like molecular pentaquarks, denoted as  $P_b$ . Several hidden-bottom pentaquarks with masses above 11 GeV and narrow widths were obtained. All of these heavy pentaquarks are worth exploring in future experiments.

**Keywords:** hidden-charm pentaquark; hidden-bottom pentaquark; scattering cross-section; quark model

**PACS:** 13.75.Cs; 12.39.Pn; 12.39.Jh



**Citation:** Zhu, X.; Wu, Y.; Huang, H.; Ping, J.; Yang, Y. Study of Hidden-Charm and Hidden-Bottom Pentaquark Resonances in the Quark Model. *Universe* **2023**, *9*, 265. <https://doi.org/10.3390/universe9060265>

Academic Editors: Roman Pasechnik and Wolfgang Schafer

Received: 24 April 2023

Revised: 18 May 2023

Accepted: 29 May 2023

Published: 31 May 2023



**Copyright:** © 2023 by the authors. Licensee MDPI, Basel, Switzerland. This article is an open access article distributed under the terms and conditions of the Creative Commons Attribution (CC BY) license (<https://creativecommons.org/licenses/by/4.0/>).

## 1. Introduction

In 2015, a report by the LHCb collaboration [1] revealed two hidden-charm pentaquark states,  $P_c(4380)$  and  $P_c(4450)$ , within the  $J/\psi p$  invariant mass spectrum of  $\Lambda_b^0 \rightarrow J/\psi K^- p$ . This has sparked interest in pentaquarks involving heavy quarks and has inspired many theoretical works on these two states, such as baryon–meson molecules [2–12], diquark–triquark pentaquarks [13,14], diquark–diquark–antiquark pentaquarks [15–18], genuine multiquark states [19], the topological soliton [20], kinematical threshold effects in the triangle singularity mechanism [21–23], and so on. Lattice QCD simulations of  $NJ/\psi$  and  $N\eta_c$  scattering were also performed to find these  $P_c$  states [24].

Four years later, the LHCb collaboration reported on three new pentaquarks, namely  $P_c(4312)$ ,  $P_c(4440)$ , and  $P_c(4457)$  [25].  $P_c(4312)$  was discovered with a significance of  $7.3\sigma$  by analyzing the  $J/\psi p$  invariant mass spectrum. The previously reported  $P_c(4450)$  structure, with a significance of  $5.4\sigma$ , was resolved into two narrow states: the  $P_c(4440)$  and  $P_c(4457)$ . The masses and widths of these states are as follows:

$$\begin{aligned}
 P_c(4312) : M &= 4311.9 \pm 0.7^{+6.8}_{-0.6} \text{ MeV}, \\
 \Gamma &= 9.8 \pm 2.7^{+3.7}_{-4.5} \text{ MeV}, \\
 P_c(4440) : M &= 4440.3 \pm 1.3^{+4.1}_{-4.7} \text{ MeV}, \\
 \Gamma &= 20.6 \pm 4.9^{+8.7}_{-10.1} \text{ MeV}, \\
 P_c(4457) : M &= 4457.3 \pm 0.6^{+4.1}_{-1.7} \text{ MeV}, \\
 \Gamma &= 6.4 \pm 2.0^{+5.7}_{-1.9} \text{ MeV}.
 \end{aligned} \tag{1}$$

As mentioned in Reference [25], because all three states are narrow and below to the  $\Sigma_c^+ \bar{D}^0$  and  $\Sigma_c^+ \bar{D}^{*0}$  thresholds within plausible hadron–hadron binding energies, they provide the strongest experimental evidence to date for the existence of molecular states composed of a charmed baryon and an anti-charmed meson. Immediately following the report by the LHCb collaboration, several theoretical studies were conducted to investigate the mass spectrum of these states [26–29]. Reference [30] investigated the isospin-breaking decays of the molecular structure of the  $P_c(4457)$ . Prior to the LHCb discovery of these two  $P_c$  states, possible hidden-charm pentaquarks were studied extensively in the frameworks of both the coupled-channel unitary approach [31] and the one-boson exchange model [32], where the existence of hidden-charm pentaquarks was predicted. More detailed information about tetraquarks and pentaquarks can be found in review articles [33–35].

Searching for the existence of multi-quark states is an important issue in hadron physics. To provide the necessary information for experiments, mass spectrum calculations alone are not sufficient. The study of hadron–hadron scattering, as well as the main production process of multi-quark states, are indispensable. As shown in Reference [25], all three new states are observed in the  $J/\psi p$  invariant mass spectrum from the  $\Lambda_b \rightarrow J/\psi p K^-$  decay, corresponding to three peaks in the  $J/\psi p$  invariant mass distributions. One common feature of the peaks is that they are all very sharp. Another important feature is that there is a two-peak structure near the mass of 4450 MeV. It is very interesting that these two peaks are located very close to each other and have similar heights, corresponding to  $P_c(4440)$  and  $P_c(4457)$ , which are split from the original  $P_c(4450)$ . In order to compare with the experimental data and investigate the properties of these peaks, we can theoretically study the cross-section of the  $J/\psi p$  scattering. If there is any resonance state during the  $J/\psi p$  scattering process, it will appear as a peak or dip in the cross-section of the  $J/\psi p$  scattering. However, in theory, due to the absence of incoherent background effects, the resonance state generally exhibits a peak on the scattering cross-section. The peak position and the half-width of the bell shape correspond to the mass and decay width of the resonance, respectively.

During the investigation of multi-quark states using various methods, QCD-inspired quark models remain the primary approach. because the direct use of quantum chromodynamics (QCD) in multi-quark states is still out of reach of the present techniques, although lattice QCD has recently made considerable progress [36]. The quark delocalization color screening model (QDCSM) [37,38] is a special version of the quark cluster model, in which two ingredients are introduced: quark delocalization (enlarges the model space) and color screening (accounts for the dependence of the quark–quark interaction on the quark state). The model has been successfully applied to describe  $NN$  and  $YN$  interactions and deuteron properties [39,40]. Dibaryon candidates, such as  $d^*$ ,  $N\Omega$ , and so on, are also studied with this model [41]. In this model, the quark delocalization, which is similar to the electron percolation in the molecules, produces an intermediate-range attraction. Color screening is needed to make the quark delocalization effective. The model provides a natural explanation for the similarity between the molecular and nuclear forces. Recently, this model has been used to study hidden-charm pentaquarks [42]; moreover, a few narrow pentaquark resonances above 4.2 GeV have been found. To investigate the three peaks in the  $J/\psi p$  invariant mass distributions in the LHCb experiment [25], we study the cross-section of the  $J/\psi p$  scattering in this work. On the one hand, we can investigate the three peaks in the  $J/\psi p$  scattering process and look for the three reported  $P_c$  states. On the other hand, we can also predict some other hidden-charm pentaquarks. Moreover, we study the hidden-bottom sector and the cross-section of  $Yp$  scattering.

The structure of this paper is as follows. A brief introduction to the quark model is given in Section 2. Section 3 is devoted to the numerical results and discussions. The last section presents the summary.

## 2. Quark Model and Wave Functions

### 2.1. The Quark Delocalization Color Screening Model

The details of QDCSM used in the present work can be found in the references [37,39]. In the following, only the Hamiltonian and parameters are given.

$$\begin{aligned}
 H &= \sum_{i=1}^5 \left( m_i + \frac{p_i^2}{2m_i} \right) - T_c + \sum_{i<j} V_{ij}, \\
 V_{ij} &= V^G(r_{ij}) + V^\chi(r_{ij}) + V^C(r_{ij}), \\
 V^G(r_{ij}) &= \frac{1}{4} \alpha_s \lambda_i \cdot \lambda_j \left[ \frac{1}{r_{ij}} - \frac{\pi}{2} \left( \frac{1}{m_i^2} + \frac{1}{m_j^2} + \frac{4\sigma_i \cdot \sigma_j}{3m_i m_j} \right) \right. \\
 &\quad \left. \delta(r_{ij}) - \frac{3}{4m_i m_j r_{ij}^3} S_{ij} \right], \\
 V^\chi(r_{ij}) &= \frac{\alpha_{ch}}{3} \frac{\Lambda^2}{\Lambda^2 - m_\chi^2} m_\chi \left\{ \left[ Y(m_\chi r_{ij}) - \frac{\Lambda^3}{m_\chi^3} Y(\Lambda r_{ij}) \right] \right. \\
 &\quad \left. \sigma_i \cdot \sigma_j + \left[ H(m_\chi r_{ij}) - \frac{\Lambda^3}{m_\chi^3} H(\Lambda r_{ij}) \right] S_{ij} \right\} \\
 &\quad \lambda_i^F \cdot \lambda_j^F, \quad \chi = \pi, K, \eta
 \end{aligned} \tag{2}$$

$$\begin{aligned}
 V^C(r_{ij}) &= -a_c \lambda_i \cdot \lambda_j [f(r_{ij}) + V_0], \\
 f(r_{ij}) &= \begin{cases} r_{ij}^2 & \text{if } i, j \text{ occur in the same} \\ & \text{baryon orbit} \\ \frac{1 - e^{-\mu_{ij} r_{ij}^2}}{\mu_{ij}} & \text{if } i, j \text{ occur in different} \\ & \text{baryon orbits} \end{cases} \\
 S_{ij} &= \frac{(\sigma_i \cdot \mathbf{r}_{ij})(\sigma_j \cdot \mathbf{r}_{ij})}{r_{ij}^2} - \frac{1}{3} \sigma_i \cdot \sigma_j.
 \end{aligned}$$

where  $T_c$  is the kinetic energy of the center of mass;  $S_{ij}$  is the quark tensor operator;  $Y(x)$  and  $H(x)$  are standard Yukawa functions [43];  $\alpha_{ch}$  is the chiral coupling constant, determined, as usual, from the  $\pi$ -nucleon coupling constant;  $\alpha_s$  is the quark–gluon coupling constant. In order to cover the broad energy range from light to heavy quarks, an effective scale-dependent quark–gluon coupling is introduced,  $\alpha_s(\mu)$  [44]:

$$\alpha_s(\mu) = \frac{\alpha_0}{\ln[(\mu^2 + \mu_0^2)/\Lambda_0^2]}, \tag{3}$$

where  $\mu$  is the reduced mass of two interacting quarks. All other symbols have their usual meanings. Moreover, a phenomenological color screening confinement potential is used, and  $\mu_{ij}$  is the color screening parameter. The light-flavor quark system is determined by fitting the deuteron properties,  $NN$  scattering phase shifts, and  $N\Lambda$  and  $N\Sigma$  scattering phase shifts, respectively, with  $\mu_{uu} = 0.45$ ,  $\mu_{us} = 0.19$ , and  $\mu_{ss} = 0.08$ , satisfying the relation  $\mu_{us}^2 = \mu_{uu} \mu_{ss}$ . When extended to the heavy quark case, we took it as an adjustable parameter,  $\mu_{cc} = 0.01 \sim 0.0001 \text{ fm}^{-2}$ , and we found that the results were not sensitive to the value of  $\mu_{cc}$ . Thus, we take parameter  $\mu_{cc} = 0.01$  in this work, and  $\mu_{uc}$  is obtained by utilizing the relation  $\mu_{uc}^2 = \mu_{uu} \mu_{cc}$ . All other parameters are taken from our previous work [6].

In QDCSM, the color screening is associated with the color structures of the system under consideration. For the three-quark baryon and quark–antiquark meson, the unscreened confinement is enough, especially for low-lying states, and the two-body interaction works

well. However, it is different in the multi-quark system. Lattice QCD calculations show string-like structures [45,46]. The confinement is a genuine multibody interaction, and, in general, one does not expect it to be described by a sum of two-body interactions. To simplify the calculations, the two-body interaction forms are still employed to evaluate the matrix elements of the Hamiltonian. The main physics introduced is the recognition that the confining interaction between two quarks in different nucleons might be different from those within one nucleon. Thus, we model the confinement as follows: the interaction is in its normal, unscreened form (quadratic in  $r_{ij}$ ) when the interacting quark pair consistently remains in the same cluster orbit before and after interaction; otherwise, the interaction takes on the screening form. Although this has not been demonstrated to be correct, it is more sophisticated than the usual, simple, two-body confining interaction; it is expected that it includes some nonlocal, non-perturbative effects of QCD, which is missing in the three-quark baryons and quark–antiquark mesons. In addition, the screened confinement permits the development of quark delocalization in the QDCSM.

The quark delocalization in QDCSM is realized by specifying the single particle orbital wave function of QDCSM as a linear combination of left and right Gaussians. More details can be seen in Equation (A15) in Appendix A, in which the mixing parameter  $\epsilon$  is not an adjusted one but is determined variationally by the dynamics of the multi-quark system itself. In this way, the multi-quark system chooses a favorable configuration in the interacting process. This mechanism has been used to explain the crossover transition between the hadron phase and quark–gluon plasma phase [47].

In this work, the resonating group method (RGM) [48], a well-established method for studying bound-state or scattering problems, is used to investigate the hidden-charm and hidden-bottom pentaquark systems. The details of RGM are shown in Appendix A.

### 2.2. Wave Functions

The orbital wave functions are shown in the appendix. The flavor, spin, and color wave functions are constructed in two steps. First, the wave functions for the meson and baryon clusters are constructed individually. Then, the wave functions of the two clusters are coupled together to form the wave function for the pentaquark system. Here, we only list the wave functions we used in this work. The flavor wave functions for a meson cluster are:

$$\chi_{I_{00}}^1 = c\bar{c}, \quad \chi_{I_{\frac{1}{2}\frac{1}{2}}}^2 = u\bar{c}, \quad \chi_{I_{\frac{1}{2}-\frac{1}{2}}}^3 = d\bar{c}. \tag{4}$$

and for a baryon cluster:

$$\begin{aligned} \chi_{I_{\frac{3}{2}\frac{3}{2}}}^4 &= \frac{1}{\sqrt{6}}(2uud - udu - duu), \\ \chi_{I_{\frac{1}{2}\frac{1}{2}}}^5 &= \frac{1}{\sqrt{2}}(udu - duu), \\ \chi_{I_{\frac{1}{2}-\frac{1}{2}}}^6 &= \frac{1}{\sqrt{6}}(-2ddu + udd + dud), \\ \chi_{I_{\frac{3}{2}-\frac{1}{2}}}^7 &= \frac{1}{\sqrt{2}}(udd - dud), \\ \chi_{I_{11}}^8 &= \frac{1}{\sqrt{6}}(2uuc - ucu - cuu), \\ \chi_{I_{11}}^9 &= \frac{1}{\sqrt{2}}(ucu - cuu), \\ \chi_{I_{10}}^{10} &= \frac{1}{\sqrt{12}}(2udc + 2duc - cdu - ucd - cud - dcu), \\ \chi_{I_{10}}^{11} &= \frac{1}{\sqrt{4}}(-cdu + ucd - cud + dcu). \end{aligned} \tag{5}$$

where the superscript of the  $\chi$  is the index of the flavor wave function for a meson or a baryon, and the subscript indicates the isospin  $I$  and the third component  $I_z$ . The spin wave functions for a meson cluster are:

$$\begin{aligned} \chi_{\sigma_{11}}^1 &= \alpha\alpha, & \chi_{\sigma_{10}}^2 &= \sqrt{\frac{1}{2}}(\alpha\beta + \beta\alpha), \\ \chi_{\sigma_{1-1}}^3 &= \beta\beta, & \chi_{\sigma_{00}}^4 &= \sqrt{\frac{1}{2}}(\alpha\beta - \beta\alpha). \end{aligned} \tag{6}$$

and for a baryon cluster are:

$$\begin{aligned} \chi_{\sigma_{\frac{3}{2}\frac{3}{2}}}^5 &= \alpha\alpha\alpha, & \chi_{\sigma_{\frac{3}{2}\frac{1}{2}}}^6 &= \frac{1}{\sqrt{3}}(\alpha\alpha\beta + \alpha\beta\alpha + \beta\alpha\alpha), \\ \chi_{\sigma_{\frac{3}{2}-\frac{1}{2}}}^7 &= \frac{1}{\sqrt{3}}(\alpha\beta\beta + \beta\beta\alpha + \beta\alpha\beta), & \chi_{\sigma_{\frac{3}{2}-\frac{3}{2}}}^8 &= \beta\beta\beta, \\ \chi_{\sigma_{\frac{1}{2}\frac{1}{2}}}^9 &= \frac{1}{\sqrt{6}}(2\alpha\alpha\beta - \alpha\beta\alpha - \beta\alpha\alpha), \\ \chi_{\sigma_{\frac{1}{2}\frac{1}{2}}}^{10} &= \frac{1}{\sqrt{2}}(\alpha\beta\alpha - \beta\alpha\alpha), \\ \chi_{\sigma_{\frac{1}{2}-\frac{1}{2}}}^{11} &= \frac{1}{\sqrt{6}}(-2\beta\beta\alpha + \alpha\beta\beta + \beta\alpha\beta), \\ \chi_{\sigma_{\frac{1}{2}-\frac{1}{2}}}^{12} &= \frac{1}{\sqrt{2}}(\alpha\beta\beta - \beta\alpha\beta). \end{aligned} \tag{7}$$

The color wave function for a meson cluster is:

$$\chi_{c[111]}^1 = \sqrt{\frac{1}{3}}(r\bar{r} + g\bar{g} + b\bar{b}). \tag{8}$$

and for a baryon cluster is:

$$\chi_{c[111]}^2 = \sqrt{\frac{1}{6}}(rgb - rbg - grb + gbr + brg - bgr). \tag{9}$$

Then, the wave functions for the pentaquark system can be obtained by coupling the wave functions of the meson and the baryon clusters. Finally, multiplying the wave functions  $\psi^L, \psi^\sigma, \psi^f$ , and  $\psi^c$ , according to the definite quantum number of the system, we can acquire the total wave functions of the system. To save space, we take the  $IJ^P = \frac{1}{2}^{\frac{1}{2}P} \Sigma_c D$  as an example. The total wave function of this state is as follows:

$$\begin{aligned} \Psi &= \mathcal{A} \left\{ \left[ \sqrt{\frac{2}{3}} \left( \sqrt{\frac{1}{2}}(\chi_{I_{11}}^8 \chi_{\sigma_{\frac{1}{2}\frac{1}{2}}}^9 + \chi_{I_{11}}^9 \chi_{\sigma_{\frac{1}{2}\frac{1}{2}}}^{10}) \chi_{I_{\frac{1}{2}-\frac{1}{2}}}^3 \chi_{\sigma_{00}}^4 \right) \right. \right. \\ &\quad \left. \left. - \sqrt{\frac{1}{3}} \left( \sqrt{\frac{1}{2}}(\chi_{I_{10}}^{10} \chi_{\sigma_{\frac{1}{2}\frac{1}{2}}}^9 + \chi_{I_{10}}^{11} \chi_{\sigma_{\frac{1}{2}\frac{1}{2}}}^{10}) \chi_{I_{\frac{1}{2}\frac{1}{2}}}^2 \chi_{\sigma_{00}}^4 \right) \right] \right. \\ &\quad \left. \cdot \chi_{c[111]}^2 \chi_{c[111]}^1 \cdot \psi^L \right\}. \end{aligned} \tag{10}$$

### 3. The Results and Discussions

In this work, we investigated the hidden-charm pentaquark resonances in the cross-section of the  $J/\psi p$  scattering. The peak position and the half-width of the bell shape correspond to the mass and the decay width of the resonance.

We calculate the cross-section of the  $J/\psi p$  scattering channel with the effect of the channel-coupling. The channels involved are listed in Table 1. The cross-section of the  $J/\psi p$  channel with  $J^P = \frac{1}{2}^-$  and  $J^P = \frac{3}{2}^-$  is shown in Figure 1. Obviously, there are four sharp peaks in the cross-section of the  $J/\psi p$  scattering, two with  $J^P = \frac{1}{2}^-$  and another two with  $J^P = \frac{3}{2}^-$ , which indicates that there are four narrow resonance states. The first one is located at a mass of 4307.9 MeV with a very narrow partial width of about 1.2 MeV. The mass is under the threshold of the  $\Sigma_c D$ , so it is the  $\Sigma_c D$  molecular pentaquark. Moreover, both the mass and decay width are close to the experimental values of the  $P_c(4312)$ , and the peak corresponds to the peak appearing in the experimental  $J/\psi p$  invariant mass distribution, which indicates that the reported  $P_c(4312)$  state could be identified as the  $\Sigma_c D$  molecular pentaquark with  $J^P = \frac{1}{2}^-$  in our model calculation.

**Table 1.** The channels involved in the calculation.

	$J^P$		Channels		
hidden charm	$\frac{1}{2}^-$	$J/\psi p$	$\Sigma_c D$	$\Sigma_c D^*$	$\Sigma_c^* D^*$
	$\frac{3}{2}^-$	$J/\psi p$	$\Sigma_c D^*$	$\Sigma_c^* D$	$\Sigma_c^* D^*$
hidden bottom	$\frac{1}{2}^-$	$\Upsilon p$	$\Sigma_b B$	$\Sigma_b B^*$	$\Sigma_b^* B^*$
	$\frac{3}{2}^-$	$\Upsilon p$	$\Sigma_b B^*$	$\Sigma_b^* B$	$\Sigma_b^* B^*$

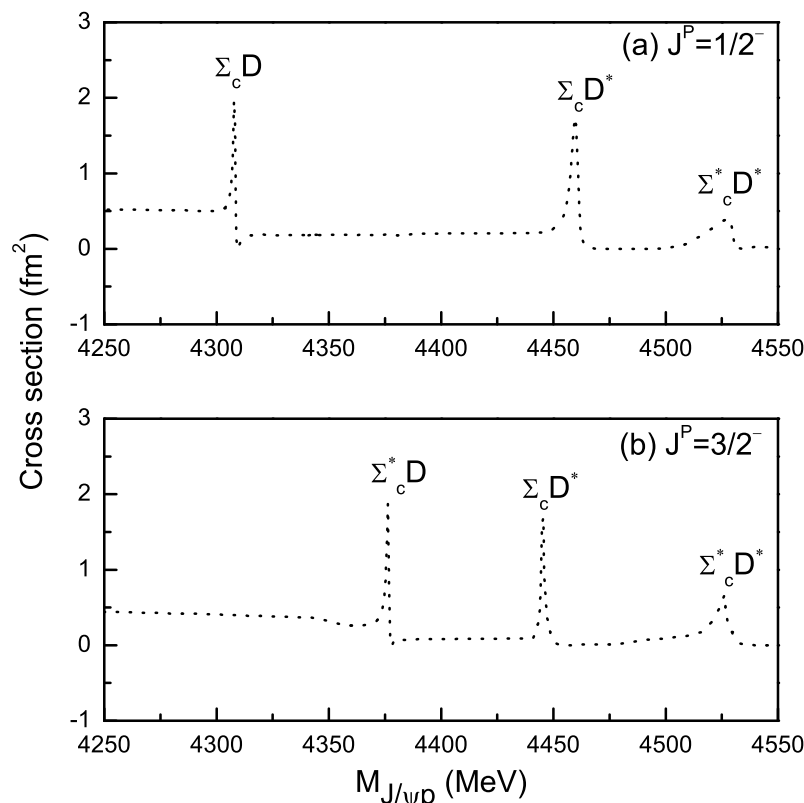


**Figure 1.** The cross-section of the  $J/\psi p$  channel with  $J^P = \frac{1}{2}^-$  and  $J^P = \frac{3}{2}^-$ , respectively.

Particularly, there are two sharp peaks in the cross-section of the  $J/\psi p$  channel near the mass of 4450 MeV. One is  $\Sigma_c D^*$  with  $J^P = \frac{1}{2}^-$ , as shown in Figure 1a, and another one is  $\Sigma_c D^*$  with  $J^P = \frac{3}{2}^-$ , as shown in Figure 1b. The masses and the partial decay widths can be seen from Figure 1; they are:  $\Sigma_c D^*$  of  $J^P = \frac{1}{2}^-$ , 4459.7 MeV, and 3.9 MeV;  $\Sigma_c D^*$  of  $J^P = \frac{3}{2}^-$ , 4445.7 MeV, and 1.5 MeV. It is obvious that these two peaks are very close to each other and have maximum cross-sections of about 2 fm<sup>2</sup>, which can reproduce a two-peak structure at about 4450 MeV, such as the one shown in the experimental  $J/\psi p$  invariant mass distribution. Compared with the experimental data, it is more likely that  $P_c(4440)$  corresponds to the molecular pentaquark  $\Sigma_c D^*$  of  $J^P = \frac{3}{2}^-$ , and  $P_c(4457)$  can be explained as the molecular pentaquark  $\Sigma_c D^*$  of  $J^P = \frac{1}{2}^-$ .

Generally, the bound state with the smaller spin should have a lower mass. It seems that this order is reversed here. This is due to the channel-coupling effect. For the  $J^P = \frac{1}{2}^-$  system, bound states exist in the single channels of  $\Sigma_c D$ ,  $\Sigma_c D^*$ , and  $\Sigma_c^* D^*$ . It may cause an increase or decrease in the mass of the  $\Sigma_c D^*$  bound state by coupling with the channels shown in Table 1; this is because there is a bound state  $\Sigma_c D$  below the  $\Sigma_c D^*$  and a  $\Sigma_c^* D^*$  bound state above the  $\Sigma_c D^*$  state. The case is similar for the  $J^P = \frac{3}{2}^-$  system. The single-channel calculation shows that the mass of  $\Sigma_c D^*$  of  $J^P = \frac{1}{2}^-$  is 4443 MeV; it is pushed up

to 4459.7 MeV by coupling with the channels shown in Table 1 because of the stronger channel-coupling effect with the lower  $\Sigma_c D$  state. Whereas the mass of the  $\Sigma_c D^*$  bound state of  $J^P = \frac{3}{2}^-$  is pushed down to 4445.7 MeV from 4451 MeV in the single-channel calculation; this is a result of the coupling with the channels listed in Table 1 due to the weaker channel-coupling effect with the lower  $\Sigma_c^* D$  state. Hence, it is understandable that the mass of the  $\Sigma_c D^*$  bound state of  $J^P = \frac{1}{2}^-$  is higher than the one of  $J^P = \frac{3}{2}^-$ . However, the mass difference is only 14 MeV here, and the model uncertainty cannot assure the mass order. Therefore, the two-peak structure can be reproduced at about 4450 MeV in our theoretical cross-section of  $J/\psi p$  scattering; these peaks arise from the resonances of  $\Sigma_c D^*$  molecular states of  $J^P = \frac{1}{2}^-$  and  $J^P = \frac{3}{2}^-$ . However, it is not easy to confirm the more exact spin parity because of the small mass difference between these two states.

Moreover, regarding the three resonances discussed above, one may see the fourth peak, as shown in Figure 1b. It is the molecular pentaquark  $\Sigma_c^* D$  with  $J^P = \frac{3}{2}^-$ . The mass of this resonance is 4376.4 MeV, which is very close to the reported  $P_c(4380)$ . However, the two-body decay width (with heavy hadron in the final state) is only 2.4 MeV, which is much smaller than the experimental value. We propose conducting an experiment to search for any narrow resonance near the  $P_c(4380)$ .

In addition, in Figure 1a, we also find that there is a cusp near the mass of 4527 MeV, which is near the threshold of the  $\Sigma_c^* D^*$ . Our previous calculation showed that the single channel  $\Sigma_c^* D^*$  state of  $J^P = \frac{1}{2}^-$  was bound, and by coupling with the  $\eta_c p$  scattering channel, the state becomes a resonance with a mass of 4525.8 MeV and width of 4.0 MeV [42]. However, it does not show up in the scattering channels  $J/\psi p$ ,  $\Sigma_c D$ , and  $\Sigma_c D^*$ , and it only appears as a cusp in the cross-section of the  $J/\psi p$  [42]. This is consistent with the experimental results; there is no distinct signal near the threshold of the  $\Sigma_c^* D^*$  in the experimental data. Moreover, there is a similar situation in the  $\Sigma_c^* D^*$  state of  $J^P = \frac{3}{2}^-$ . It appears as a resonance with a mass of 4523.0 MeV and width of 1.0 MeV in the  $\Lambda_c D^*$  scattering process, but it only showed up as a cusp in the cross-section of the  $J/\psi p$  (see Figure 1b) [42]. Although it is difficult for the experiment to perform the  $\eta_c p$  or the  $\Lambda_c D^*$  scattering, the  $\Sigma_c^* D^*$  of both  $J^P = \frac{1}{2}^-$  and  $J^P = \frac{3}{2}^-$  are possible molecular pentaquarks, which are worth looking for.

Because of the heavy flavor symmetry, we also extend the study to the hidden-bottom pentaquarks. The results are similar to the hidden-charm molecular pentaquarks. Figure 2 shows the cross-sections of the  $Yp$  channel with  $J^P = \frac{1}{2}^-$  and  $J^P = \frac{3}{2}^-$ , respectively. From Figure 2a, we can see three sharp peaks in the cross-sections, which correspond to three resonance states, i.e.,  $\Sigma_b B$ ,  $\Sigma_b B^*$ , and  $\Sigma_b^* B^*$ , with  $J^P = \frac{1}{2}^-$ . The resonance mass of the  $\Sigma_b B$  state is 11,077.5 MeV and the decay width is about 0.1 MeV;  $\Sigma_b B^*$  has a mass of 11,125.8 MeV and a decay width of 0.8 MeV; and  $\Sigma_b^* B^*$  has a mass of 11,153.5 MeV and a decay width of 3.0 MeV.

For the hidden-bottom pentaquarks with  $J^P = \frac{3}{2}^-$ , two pinnacles appear in the Figure 2b, corresponding to two resonance states:  $\Sigma_b^* B$  and  $\Sigma_b B^*$ . The mass and the decay width of  $\Sigma_b^* B$  are 11,103.6 MeV and 0.8 MeV, respectively. The mass and the decay width of  $\Sigma_b B^*$  are 11,122.7 MeV and 0.2 MeV, respectively. Moreover, there is only a cusp around the threshold of the third state,  $\Sigma_b^* B^*$ . The reason is that the coupling with the channel pushes the higher state above the threshold. All of these hidden-bottom pentaquarks have similar properties with hidden-charm pentaquarks, so we can call them  $P_c$ -like molecular pentaquarks  $P_b$ , which are also worth investigating in experiments. In particular, the nature of these hidden-charm and hidden-bottom pentaquarks is similar to the corresponding  $N_{cc}^*$  and  $N_{bb}^*$  states predicated in References [49,50], which definitely cannot be accommodated by the conventional  $3q$  quark models, and should form part of the heavy island for the quite stable  $N^*$  baryons.

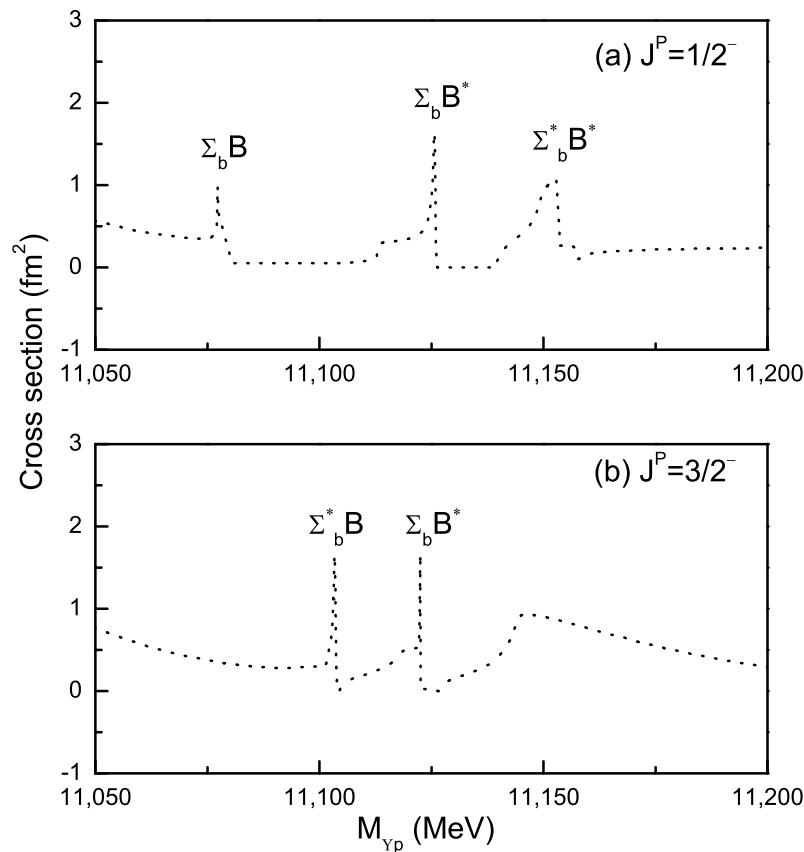


**Figure 2.** The cross-section of the  $Yp$  channel with  $J^P = \frac{1}{2}^-$  and  $J^P = \frac{3}{2}^-$ , respectively.

#### 4. Summary

To summarize, our study is inspired by the observation of three narrow pentaquarks, namely  $P_c(4312)$ ,  $P_c(4440)$ , and  $P_c(4457)$ , observed in the process  $\Lambda_b^0 \rightarrow J/\psi K^- p$ , as reported by LHCb. We investigated the cross-section of  $J/\psi p$  scattering in the quark delocalization color screening model. Four peaks were found in the cross-section. The mass and width of the first one was close to the  $P_c(4312)$ , which indicates that the  $P_c(4312)$  can be interpreted as the hidden-charm molecular pentaquark  $\Sigma_c D$  with  $J^P = \frac{1}{2}^-$ . The two-peak structure can be reproduced at about 4450 MeV in our theoretical cross-section of  $J/\psi p$  scattering, corresponding to  $P_c(4440)$  and  $P_c(4457)$ . They correspond to the resonances of the molecular pentaquarks  $\Sigma_c D^*$  of  $J^P = \frac{1}{2}^-$  and  $J^P = \frac{3}{2}^-$ . The more exact spin parity should be confirmed through both theoretical and experimental studies in the future. Another molecular pentaquark  $\Sigma_c^* D$  with  $J^P = \frac{3}{2}^-$  is also suggested in our calculation, the mass of which is close to the  $P_c(4380)$ , but with a width much smaller than it. Moreover, the  $\Sigma_c^* D^*$  of both  $J^P = \frac{1}{2}^-$  and  $J^P = \frac{3}{2}^-$  are possible molecular pentaquarks. All of these narrow pentaquarks are worth searching for or will be confirmed in future experiments.

Note that all of the  $P_c$  state measurements have been made by LHCb. The only independent evidence for the  $P_c$  states to date comes from the D0 collaboration, which observes events that are consistent with the unresolved  $P_c(4440) \rightarrow J/\psi p$  structure at  $3.2\sigma$  [51]. The gluonic excitation (GlueX) experiment measured the total cross-sections for the reaction  $\gamma p \rightarrow J/\psi p$  and reported no evidence for the LHCb pentaquark candidates  $P_c$  [52]. New higher-statistic GlueX measurements of the threshold's total cross-section, for the reaction  $\gamma p \rightarrow J/\psi p$  [53], motivated an alternative search for the LHCb exotics. There is still much that remains unknown about the pentaquark states. Higher statistics data and more theoretical works in the future might provide more information for the hidden-heavy flavor pentaquark states. CLAS12 at Jefferson Lab (JLab) may be a possible place to observe the  $P_c$  states in  $J/\psi$  photoproduction [54,55]. Its spin and photocoupler may be measured

with future data, too. The search for the LHCb pentaquark in the photo-production process at Hall C, JLab, has received approval [56]. Moreover, pentaquarks with charm quarks can also be observed by the PANDA/FAIR [57].

For hidden-bottom pentaquarks, we predict several  $P_c$ -like molecular pentaquarks  $P_b$  above 11 GeV with narrow widths in the  $Yp$  scattering process. We hope that the proposed electron-ion collider (EIC) [58] and the upgraded facilities at JLab [59] can play important roles in discovering these interesting super-heavy pentaquarks.

**Author Contributions:** Conceptualization, H.H. and J.P.; methodology, J.P.; software, X.Z.; validation, Y.W. and Y.Y.; formal analysis, X.Z.; investigation, X.Z.; resources, Y.Y.; data curation, Y.W.; writing—original draft preparation, X.Z.; writing—review and editing, H.H.; visualization, Y.Y.; supervision, J.P.; project administration, H.H.; funding acquisition, J.P. All authors have read and agreed to the published version of the manuscript

**Funding:** This work is supported partly by the National Natural Science Foundation of China under contract nos. 11675080, 11775118, 11535005, and 11865019.

**Data Availability Statement:** This manuscript has no associated data or the data will not be deposited.

**Conflicts of Interest:** The authors declare no conflict of interest.

### Appendix A. Resonating Group Method for Bound-State and Scattering Problems

We use the resonating group method (RGM) to carry out a dynamic calculation. For a bound-state problem; we write the wave function of the baryon-meson system as

$$\Psi_{5q} = \mathcal{A} \sum_L \left[ [\hat{\phi}_A(\rho_A, \lambda_A) \hat{\phi}_B(\rho_B)]^{[\sigma]IS} \otimes \chi_L(\mathbf{R}) \right]^J. \tag{A1}$$

where  $[\sigma] = [222]$  gives the total color symmetry and all other symbols have their usual meanings. The symbol  $\mathcal{A}$  is the anti-symmetrization operator. With the  $SU(4)$  extension, both the light and heavy quarks are considered identical particles. Thus,  $\mathcal{A}$  is written as

$$\mathcal{A} = 1 - P_{14} - P_{24} - P_{34}. \tag{A2}$$

where 1, 2, and 3 stand for the quarks in the baryon cluster, and 4 stands for the quark in the meson cluster.  $\hat{\phi}_A$  and  $\hat{\phi}_B$  are the anti-symmetrized internal cluster wave functions of the baryon A and meson B:

$$\hat{\phi}_A(\rho_A, \lambda_A) = \left(\frac{2}{3\pi b^2}\right)^{3/4} \left(\frac{1}{2\pi b^2}\right)^{3/4} e^{-\left(\frac{\lambda_A^2}{3b^2} + \frac{\rho_A^2}{4b^2}\right)} \eta_{I_A S_A} \chi_c(A), \tag{A3}$$

$$\hat{\phi}_B(\rho_B) = \left(\frac{1}{2\pi b^2}\right)^{3/4} e^{-\frac{\rho_B^2}{4b^2}} \eta_{I_B S_B} \chi_c(B). \tag{A4}$$

where  $\eta_{I_A S_A}$  and  $\chi_c(A)$  are the internal flavor-spin and color wave functions of the baryon cluster A. The Jacobi coordinates are defined as follows:

$$\begin{aligned} \rho_A &= \mathbf{r}_1 - \mathbf{r}_2, & \rho_B &= \mathbf{r}_4 - \mathbf{r}_5, \\ \lambda_A &= \mathbf{r}_3 - \frac{1}{2}(\mathbf{r}_1 + \mathbf{r}_2), \\ \mathbf{R}_A &= \frac{1}{3}(\mathbf{r}_1 + \mathbf{r}_2 + \mathbf{r}_3), & \mathbf{R}_B &= \frac{1}{2}(\mathbf{r}_4 + \mathbf{r}_5), \\ \mathbf{R} &= \mathbf{R}_A - \mathbf{R}_B, & \mathbf{R}_G &= \frac{3}{5}\mathbf{R}_A + \frac{2}{5}\mathbf{R}_B. \end{aligned} \tag{A5}$$

From the variational principle, after variation with respect to the relative motion wave function  $\chi(\mathbf{R}) = \sum_L \chi_L(\mathbf{R})$ , one obtains the following RGM equation

$$\int H(\mathbf{R}'', \mathbf{R}') \chi(\mathbf{R}') d\mathbf{R}' = E \int N(\mathbf{R}'', \mathbf{R}') \chi(\mathbf{R}') d\mathbf{R}', \tag{A6}$$

where the Hamiltonian kernel  $H(\mathbf{R}'', \mathbf{R}')$  and normalization kernel  $N(\mathbf{R}'', \mathbf{R}')$  can, respectively, be calculated by

$$\left\{ \begin{matrix} H(\mathbf{R}'', \mathbf{R}') \\ N(\mathbf{R}'', \mathbf{R}') \end{matrix} \right\} = \left\langle \mathcal{A}[\hat{\phi}_A(\rho_A, \lambda_A) \hat{\phi}_B(\rho_B) \delta(\mathbf{R} - \mathbf{R}'')] \right. \\ \left. \left| \left\{ \begin{matrix} H \\ 1 \end{matrix} \right\} \right| \mathcal{A}[\hat{\phi}_A(\rho_A, \lambda_A) \hat{\phi}_B(\rho_B) \delta(\mathbf{R} - \mathbf{R}')] \right\rangle. \tag{A7}$$

For a bound-state problem, the energies and the wave functions  $\chi(\mathbf{R})$  are obtained by solving the RGM equation. In practice, it is not convenient to work with the RGM expressions. We introduce generator coordinates  $S_i$  to expand the  $L$ th relative motion wave function  $\chi_L(\mathbf{R})$ :

$$\chi_L(\mathbf{R}) = \frac{1}{\sqrt{4\pi}} \left(\frac{6}{5\pi b^2}\right)^{3/4} \sum_{i=1}^n C_i \\ \times \int \exp\left[-\frac{3}{5b^2}(\mathbf{R} - S_i)^2\right] Y^L(\hat{S}_i) d\hat{S}_i \\ = \sum_{i=1}^n C_i \frac{u_L(R, S_i)}{R} Y^L(\hat{\mathbf{R}}), \tag{A8}$$

with

$$u_L(R, S_i) = \sqrt{4\pi} \left(\frac{6}{5\pi b^2}\right)^{3/4} R \\ \times \exp\left[-\frac{3}{5b^2}(R^2 - S_i^2)\right] i^L j_L(-i\frac{6}{5b^2}RS_i). \tag{A9}$$

where  $C_i$  represents the expansion coefficients,  $n$  represents the number of Gaussian bases, which is determined by the stability of the results, and  $j_L$  represents the  $L$ th spherical Bessel function. Then the relative motion wave function  $\chi(\mathbf{R})$  is

$$\chi(\mathbf{R}) = \frac{1}{\sqrt{4\pi}} \sum_L \left(\frac{6}{5\pi b^2}\right)^{3/4} \sum_{i=1}^n C_{i,L} \\ \times \int e^{-\frac{3}{5b^2}(\mathbf{R}-S_i)^2} Y^L(\hat{S}_i) d\Omega_{S_i}. \tag{A10}$$

After including the motion of the center of mass,

$$\Phi_G(\mathbf{R}_G) = \left(\frac{5}{\pi b^2}\right)^{3/4} e^{-\frac{5}{2b^2}\mathbf{R}_G^2}, \tag{A11}$$

the total wave function Equation (A1) can be rewritten as

$$\Psi_{5q} = \mathcal{A} \sum_{i,L} C_{i,L} \int \frac{d\Omega_{S_i}}{\sqrt{4\pi}} \prod_{\alpha=1}^3 \phi_{\alpha}(S_i) \prod_{\beta=4}^5 \phi_{\beta}(-S_i) \\ \times \left[ [\eta_{I_A S_A} \eta_{I_B S_B}]^{IS} Y^L(\hat{S}_i) \right]^J [\chi_c(A) \chi_c(B)]^{[\sigma]}. \tag{A12}$$

where  $\phi_\alpha(\mathbf{S}_i)$  and  $\phi_\beta(-\mathbf{S}_i)$  are the single-particle orbital wave functions with different reference centers:

$$\begin{aligned} \phi_\alpha(\mathbf{S}_i) &= \left(\frac{1}{\pi b^2}\right)^{3/4} e^{-\frac{1}{2b^2}(r_\alpha - \frac{2}{3}\mathbf{S}_i)^2}, \\ \phi_\beta(-\mathbf{S}_i) &= \left(\frac{1}{\pi b^2}\right)^{3/4} e^{-\frac{1}{2b^2}(r_\beta + \frac{3}{5}\mathbf{S}_i)^2}. \end{aligned} \tag{A13}$$

With the reformulated Equation (A12), the RGM Equation (A6) becomes an algebraic eigenvalue equation:

$$\sum_{j,L} C_{j,L} H_{ij}^{L,L'} = E \sum_j C_{j,L'} N_{ij}^{L'} \tag{A14}$$

where  $N_{ij}^{L'}$  and  $H_{ij}^{L,L'}$  are the wave function (A12) overlaps and Hamiltonian matrix elements (without the summation over  $L'$ ), respectively. By solving the generalized eigenproblem, we obtain the energies of the 5-quark systems and their corresponding wave functions. In our calculation, the Gaussian distribution is chosen to ensure the stability of the results. If the numerical results stabilize as the size of the space and the number of Gaussians increase, it indicates that they have converged to the true energies of the Hamiltonian. In the present work, the results are stable when the largest distance between the baryon and meson clusters is around 6 fm. To keep the matrix dimensions manageable, the baryon-meson separation is taken to be less than 6 fm.

In the QDCSM, the single-particle orbital wave functions are delocalized. To implement this here, we modify Equation (A13) as follows:

$$\begin{aligned} \phi_\alpha(\mathbf{S}_i) \rightarrow \psi_\alpha(\mathbf{S}_i, \epsilon) &= (\phi_\alpha(\mathbf{S}_i) + \epsilon\phi_\alpha(-\mathbf{S}_i))/N(\epsilon), \\ \phi_\beta(\mathbf{S}_i) \rightarrow \psi_\beta(\mathbf{S}_i, \epsilon) &= (\phi_\beta(\mathbf{S}_i) + \epsilon\phi_\beta(-\mathbf{S}_i))/N(\epsilon), \\ N(\epsilon) &= \sqrt{1 + \epsilon^2 + 2\epsilon e^{-S_i^2/4b^2}}. \end{aligned} \tag{A15}$$

For a scattering problem, the relative wave function is expanded as

$$\chi_L(\mathbf{R}) = \sum_{i=1}^n C_i \frac{\tilde{u}_L(R, S_i)}{R} Y^L(\hat{\mathbf{R}}). \tag{A16}$$

with

$$\tilde{u}_L(R, S_i) = \begin{cases} \alpha_i u_L(R, S_i), & R \leq R_C \\ [h_L^-(k, R) - s_i h_L^+(k, R)] R, & R \geq R_C \end{cases} \tag{A17}$$

where  $u_L$  is from Equation (A9),  $h_L^\pm$  represents the  $L$ th spherical Hankel functions,  $k$  is the momentum of relative motion, calculated as  $k = \sqrt{2\mu E_{cm}}$ ,  $\mu$  is the reduced mass of two hadrons (A and B) in the open channel,  $E_{cm}$  is the incident energy, and  $R_C$  is the cutoff radius beyond which all strong interactions can be disregarded. Moreover,  $\alpha_i$  and  $s_i$  are complex parameters that are determined by the smoothness condition at  $R = R_C$ , and  $C_i$  satisfies  $\sum_{i=1}^n C_i = 1$ . After performing the variational procedure, an  $L$ th partial-wave equation for the scattering problem can be deduced as

$$\sum_{j=1}^n \mathcal{L}_{ij}^L C_j = \mathcal{M}_i^L \quad (i = 0, 1, \dots, n - 1), \tag{A18}$$

with

$$\mathcal{L}_{ij}^L = \mathcal{K}_{ij}^L - \mathcal{K}_{i0}^L - \mathcal{K}_{0j}^L + \mathcal{K}_{00}^L, \tag{A19}$$

$$\mathcal{M}_i^L = \mathcal{K}_{00}^L - \mathcal{K}_{i0}^L, \tag{A20}$$

and

$$\mathcal{K}_{ij}^L = \left\langle \hat{\phi}_A \hat{\phi}_B \frac{\tilde{u}_L(R', S_i)}{R'} Y^L(\hat{\mathbf{R}}') | H - E | \mathcal{A} \left[ \hat{\phi}_A \hat{\phi}_B \frac{\tilde{u}_L(R, S_j)}{R} Y^L(\hat{\mathbf{R}}) \right] \right\rangle. \tag{A21}$$

By solving Equation (A18), we can obtain the expansion coefficients  $C_i$ . Then the  $S$ -matrix element  $S_L$  and the phase shifts  $\delta_L$  are given by

$$S_L \equiv e^{2i\delta_L} = \sum_{i=1}^n C_i s_i. \tag{A22}$$

Finally, the cross-section can be obtained from the scattering phase shifts by the following formula:

$$\sigma_L = \frac{4\pi}{k^2} \cdot (2L + 1) \cdot \sin^2 \delta_L. \tag{A23}$$

### References

1. Aaij, R.; Adeva, B.; Adinolfi, M.; Affolder, A.; Ajaltouni, Z.; Akar, S.; Albrecht, J.; Alessio, F.; Alexander, M.; Ali, S.; et al. Observation of  $J/\psi p$  resonances consistent with pentaquark states in  $\Lambda_b^0 \rightarrow J/\psi K^- p$  decays. *Phys. Rev. Lett.* **2015**, *115*, 072001.
2. Chen, R.; Liu, X.; Li, X.Q.; Zhu, S.L. Identifying exotic hidden-charm pentaquarks. *Phys. Rev. Lett.* **2015**, *115*, 132002. [[CrossRef](#)] [[PubMed](#)]
3. Chen, H.X.; Chen, W.; Liu, X.; Steele, T.G.; Zhu, S.L. Towards exotic hidden-charm pentaquarks in QCD. *Phys. Rev. Lett.* **2015**, *115*, 172001. [[CrossRef](#)]
4. Roca, L.; Nieves, J.; Oset, E. LHCb pentaquark as a  $\bar{D}^* \Sigma_c - \bar{D}^* \Sigma_c^*$  molecular state. *Phys. Rev. D* **2015**, *92*, 094003. [[CrossRef](#)]
5. He, J.  $\bar{D} \Sigma_c^*$  and  $\bar{D}^* \Sigma_c$  interactions and the LHCb hidden-charmed pentaquarks. *Phys. Lett. B* **2016**, *753*, 547–551. [[CrossRef](#)]
6. Huang, H.X.; Deng, C.R.; Ping, J.L.; Wang, F. Possible pentaquarks with heavy quarks. *Eur. Phys. J. C* **2016**, *76*, 624. [[CrossRef](#)]
7. Yang, G.; Ping, J.L.; Wang, F. The structure of pentaquarks  $P_c^+$  in the chiral quark model. *Phys. Rev. D* **2017**, *95*, 014010. [[CrossRef](#)]
8. Meissner, U.G.; Oller, J.A. Testing the  $\chi_{c1} p$  composite nature of the  $P_c(4450)$ . *Phys. Lett. B* **2015**, *751*, 59–62. [[CrossRef](#)]
9. Xiao, C.W.; Meissner, U.G.  $J/\psi(\eta c)N$  and  $Y(\eta b)N$  cross-sections. *Phys. Rev. D* **2015**, *92*, 114002. [[CrossRef](#)]
10. Chen, R.; Liu, X.; Zhu, S.L. Hidden-charm molecular pentaquarks and their charm-strange partners. *Nucl. Phys. A* **2016**, *954*, 406–421. [[CrossRef](#)]
11. Chen, H.X.; Cui, E.L.; Chen, W.; Liu, X.; Steele, T.G.; Zhu, S.L. QCD sum rule study of hidden-charm pentaquarks. *Eur. Phys. J. C* **2016**, *76*, 572. [[CrossRef](#)]
12. Azizi, K.; Sarac, Y.; Sundu, H. Analysis of  $P_c^+(4380)$  and  $P_c^+(4450)$  as pentaquark states in the molecular picture with QCD sum rules. *Phys. Rev. D* **2017**, *95*, 094016. [[CrossRef](#)]
13. Lebed, R.F. The pentaquark candidates in the dynamical diquark picture. *Phys. Lett. B* **2015**, *749*, 454–457. [[CrossRef](#)]
14. Zhu, R.L.; Qiao, C.F. Pentaquark states in a diquark–triquark model. *Phys. Lett. B* **2016**, *756*, 259–264. [[CrossRef](#)]
15. Maiani, L.; Polosa, A.D.; Riquer, V. The new pentaquarks in the diquark model. *Phys. Lett. B* **2015**, *749*, 289–291. [[CrossRef](#)]
16. Anisovich, V.V.; Matveev, M.A.; Nyiri, J.; Sarantsev, A.V.; Semenova, A.N. Pentaquarks and resonances in the  $pJ/\psi$  spectrum. *arXiv* **2015**, arXiv:1507.07652.
17. Ghosh, R.; Bhattacharya, A.; Chakrabarti, B. A study on  $P_c^*(4380)$  and  $P_c^*$  in the quasi particle diquark model. *Phys. Part. Nucl. Lett.* **2017**, *14*, 550–552. [[CrossRef](#)]
18. Wang, Z.G. Analysis of  $P_c(4380)$  and  $P_c(4450)$  as pentaquark states in the diquark model with QCD sum rules. *Eur. Phys. J. C* **2016**, *76*, 70. [[CrossRef](#)]
19. Mironov, A.; Morozov, A. Is the pentaquark doublet a hadronic molecule? *JETP Lett.* **2015**, *102*, 271–273. [[CrossRef](#)]
20. Scoccola, N.N.; Riska, D.O.; Rho, M. Pentaquark candidates  $P_c^+(4380)$  and  $P_c^+(4450)$  within the soliton picture of baryons. *Phys. Rev. D* **2015**, *92*, 051501. [[CrossRef](#)]
21. Guo, F.K.; Meissner, U.G.; Wang, W.; Yang, Z. How to reveal the exotic nature of the  $P_c(4450)$ . *Phys. Rev. D* **2015**, *92*, 071502. [[CrossRef](#)]
22. Liu, X.H.; Wang, Q.; Zhao, Q. Understanding the newly observed heavy pentaquark candidates. *Phys. Lett. B* **2016**, *757*, 231–236. [[CrossRef](#)]
23. Mikhasenko, M. A triangle singularity and the LHCb pentaquarks. *arXiv* **2015**, arXiv:1507.06552.
24. Skerbis, U.; Prelovsek, S. Nucleon- $J/\psi$  and nucleon- $\eta_c$  scattering in  $P_c$  pentaquark channels from LQCD. *Phys. Rev. D* **2019**, *99*, 094505. [[CrossRef](#)]
25. Aaij, R.; Abellan Beteta, C.; Adeva, B.; Adinolfi, M.; Aidala, C.A.; Ajaltouni, Z.; Akar, S.; Albicocco, P.; Albrecht, J.; Alessio, F.; et al. Observation of a narrow pentaquark state,  $P_c(4312)^+$ , and of two-peak structure of the  $P_c(4450)^+$ . *Phys. Rev. Lett.* **2019**, *122*, 222001. [[PubMed](#)]

26. Chen, H.X.; Chen, W.; Zhu, S.L. Possible interpretations of the  $P_c(4312)$ ,  $P_c(4440)$ , and  $P_c(4457)$ . *Phys. Rev. D* **2019**, *100*, 051501. [[CrossRef](#)]
27. Chen, R.; Sun, Z.F.; Liu, X.; Zhu, S.L. Strong LHCb evidence supporting the existence of the hidden-charm molecular pentaquarks. *Phys. Rev. D* **2019**, *100*, 011502. [[CrossRef](#)]
28. Liu, M.Z.; Pan, Y.W.; Peng, F.Z.; Sanchez, M.S.; Geng, L.S.; Hosaka, A.; Valderrama, P. Emergence of a complete heavy-quark spin symmetry multiplet: Seven molecular pentaquarks in light of the latest LHCb analysis. *Phys. Rev. Lett.* **2019**, *122*, 242001. [[CrossRef](#)]
29. He, J. Study of  $P_c(4457)$ ,  $P_c(4440)$ , and  $P_c(4312)$  in a quasipotential Bethe-Salpeter equation approach. *Eur. Phys. J. C* **2019**, *79*, 393. [[CrossRef](#)]
30. Guo, F.K.; Jing, H.J.; Meissner, U.-G.; Sakai, S. Isospin breaking decays as a diagnosis of the hadronic molecular structure of the  $P_c(4457)$ . *Phys. Rev. D* **2019**, *99*, 091501. [[CrossRef](#)]
31. Wu, J.J.; Molina, R.; Oset, E.; Zou, B.S. Prediction of narrow  $N^*$  and  $\Lambda^*$  resonances with hidden charm above 4 GeV. *Phys. Rev. Lett.* **2010**, *105*, 232001. [[CrossRef](#)]
32. Yang, Z.C.; Sun, Z.F.; He, J.; Liu, X.; Zhu, S.L. The possible hidden-charm molecular baryons composed of anti-charmed meson and charmed baryon. *Chin. Phys. C* **2012**, *36*, 6–13. [[CrossRef](#)]
33. Chen, H.X.; Chen, W.; Liu, X.; Zhu, S.L. The hidden-charm pentaquark and tetraquark states. *Phys. Rep.* **2016**, *639*, 1–121. [[CrossRef](#)]
34. Liu, Y.R.; Chen, H.X.; Chen, W.; Liu, X.; Zhu, S.L. Pentaquark and tetraquark states. *Prog. Part. Nucl. Phys.* **2019**, *107*, 237–320. [[CrossRef](#)]
35. Yang, G.; Ping, J.L.; Segovia, J. Tetra- and penta-quark structures in the constituent quark model. *Symmetry* **2020**, *12*, 1869. [[CrossRef](#)]
36. Aoki, S. Nucleon-nucleon interactions via Lattice QCD: Methodology: HAL QCD approach to extract hadronic interactions in lattice QCD. *Eur. Phys. J. A* **2013**, *49*, 81. [[CrossRef](#)]
37. Wang, F.; Wu, G.H.; Teng, L.J.; Goldman, T. Quark delocalization, color screening, and nuclear intermediate range attraction. *Phys. Rev. Lett.* **1992**, *69*, 2901–2904. [[CrossRef](#)] [[PubMed](#)]
38. Wu, G.H.; Teng, L.J.; Ping, J.L.; Wang, F.; Goldman, T. Quark delocalization, color screening, and NN intermediate range attraction: P waves. *Phys. Rev. C* **1996**, *53*, 1161–1166. [[CrossRef](#)] [[PubMed](#)]
39. Ping, J.L.; Wang, F.; Goldman, T. Effective baryon baryon potentials in the quark delocalization and color screening model. *Nucl. Phys. A* **1999**, *657*, 95–109. [[CrossRef](#)]
40. Wu, G.H.; Ping, J.L.; Teng, L.J.; Wang, F.; Goldman, T. Quark delocalization, color screening model and nucleon baryon scattering. *Nucl. Phys. A* **2000**, *673*, 279–297. [[CrossRef](#)]
41. Ping, J.L.; Huang, H.X.; Pang, H.R.; Wang, F.; Wong, C.W. Quark models of dibaryon resonances in nucleon-nucleon scattering. *Phys. Rev. C* **2009**, *79*, 024001. [[CrossRef](#)]
42. Huang, H.X.; Ping, J.L. Investigating the hidden-charm and hidden-bottom pentaquark resonances in scattering process. *Phys. Rev. D* **2019**, *99*, 014010. [[CrossRef](#)]
43. Valcarce, A.; Garcilazo, H.; Fernandez, F.; Gonzalez, P. Quark-model study of few-baryon systems. *Rep. Prog. Phys.* **2005**, *68*, 965–1042. [[CrossRef](#)]
44. Vijande, J.; Fernandez, F.; Valcarce, A. Constituent quark model study of the meson spectra. *J. Phys. G* **2005**, *31*, 481. [[CrossRef](#)]
45. Laermann, E.; Langhammer, F.; Schmitt, I.; Zerwas, P.M. The interquark potential: SU(2) color gauge theory with fermions. *Phys. Lett. B* **1986**, *173*, 437–442. [[CrossRef](#)]
46. Born, K.D.; Laermann, E.; Pirch, N.; Walsh, T.F.; Zerwas, P.M. Hadron properties in lattice QCD with dynamical fermions. *Phys. Rev. D* **1989**, *40*, 1653–1663. [[CrossRef](#)]
47. Xu, M.M.; Yu, M.L.; Liu, L.S. Examining the crossover from hadronic to partonic phase in QCD. *Phys. Rev. Lett.* **2008**, *100*, 092301. [[CrossRef](#)]
48. Kamimura, M. Chapter V. A Coupled Channel Variational Method for Microscopic Study of Reactions between Complex Nuclei. *M. Suppl. Prog. Theor. Phys.* **1977**, *62*, 236. [[CrossRef](#)]
49. Wu, J.J.; Molina, R.; Oset, E.; Zou, B.S. Dynamically generated  $N^*$  and  $\Lambda^*$  resonances in the hidden charm sector around 4.3 GeV. *Phys. Rev. C* **2011**, *84*, 015202.
50. Wu, J.J.; Zhao, L.; Zou, B.S. Prediction of super-heavy  $N^*$  and  $\Lambda^*$  resonances with hidden beauty. *Phys. Lett. B* **2012**, *709*, 70–76. [[CrossRef](#)]
51. Abazov, V.M.; Abbott, B.; Acharya, B.S.; Adams, M.; Adams, T.; Agnew, J.P.; Alexeev, G.D.; Alkhazov, G.; Altona, A.; Askew, A.; et al. Inclusive production of the  $P_c$  resonances in  $p\bar{p}$  collisions. *arXiv* **2019**, arXiv:1910.11767.
52. Ali, A.; Amaryan, M.; Anassontzis, E.G.; Austregesilo, A.; Baalouch, M.; Barbosa, F.; Barlow, J.; Barnes, A.; Barriga, E.; Beattie, T.D.; et al. First Measurement of Near-Threshold  $J/\psi$  Exclusive Photoproduction off the Proton. *Phys. Rev. Lett.* **2019**, *123*, 072001. [[CrossRef](#)] [[PubMed](#)]
53. Adhikari, S.; Afzal, F.; Akondi, C.S.; Albrecht, M.; Amaryan, M.; Arroyave, V.; Asaturyan, A.; Austregesilo, A.; Baldwin, Z.; Barbosa, F.; et al. Measurement of the  $J/\psi$  photoproduction cross-section over the full near-threshold kinematic region. *arXiv* **2023**, arXiv:2304.03845.

54. Hiller Blin, A.N.; Fernandez-Ramirez, C.; Jackura, A.; Mathieu, V.; Mokeev, V.I.; Pilloni, A.; Szczepaniak, A.P. Studying the  $P_c(4450)$  resonance in  $J/\psi$  photoproduction off protons. *Phys. Rev. D* **2016**, *94*, 034002.
55. Kubarovsky, V.; Voloshin, M.B. Search for hidden-charm pentaquark with CLAS12. *arXiv* **2016**, arXiv:1609.00050.
56. Meizianin, Z.E.; Joosten, S.; Paolonen, M.; Chudakov, E.; Jones, M.; Adhikari, K.; Aniol, K.; Armstrong, W.; Arrington, J.; Asaturyan, A.; et al. A Search for the LHCb charmed 'pentaquark' using photo-production of  $J/\psi$  at threshold in Hall C at Jefferson Lab. *arXiv* **2016**, arXiv:1609.00676.
57. Erni, W.; Keshelashvili, I.; Krusche, B.; Steinacher, M.; Heng, Y.; Liu, Z.; Liu, H.; Shen, X.; Wang, O.; Xu, H.; et al. Physics Performance Report for PANDA: Strong Interaction Studies with Antiprotons. *arXiv* **2009**, arXiv:0903.3905.
58. Ptitsyn, V. Polarized beams at EICs. *AIP Conf. Proc.* **2009**, *1149*, 735–740.
59. Joosten, S.; Meiziani, Z.E. Heavy quarkonium production at threshold: From JLab to EIC. *arXiv* **2018**, arXiv:1802.02616.

**Disclaimer/Publisher's Note:** The statements, opinions and data contained in all publications are solely those of the individual author(s) and contributor(s) and not of MDPI and/or the editor(s). MDPI and/or the editor(s) disclaim responsibility for any injury to people or property resulting from any ideas, methods, instructions or products referred to in the content.